ADVANCED OPTICAL MATERIALS

Supporting Information

for *Adv. Optical Mater.,* DOI: 10.1002/adom.202203096

Efficient Ligand Passivation Enables Ultrastable $CsPbX_3$ Perovskite Nanocrystals in Fully Alcohol Environments

Andrés F. Gualdrón-Reyes, Roser Fernández-Climent, Sofia Masi, Camilo A. Mesa, Carlos Echeverría-Arrondo, Federica Aiello, Federica Balzano, Gloria Uccello-Barretta, Jhonatan Rodríguez-Pereira, Sixto Giménez, and Iván Mora-Seró**

Supporting Information

Efficient Ligand Passivation Enables Ultrastable $CsPbX_3$ Perovskite Nanocrystals in Fully Alcohol Environments

Andrés F. Gualdrón-Reyes,[1,2,*] Roser Fernández-Climent,[1] Sofia Masi,[1] Camilo A. Mesa,[1] Carlos Echeverría-Arrondo,[1] Federica Aiello,[3] Federica Balzano,[4] Gloria Uccello-Barretta,[4] Jhonatan Rodríguez-Pereira,[5,6] Sixto Giménez[1] and Iván Mora-Seró[1,*]

[1]Institute of Advanced Materials (INAM), Universitat Jaume I (UJI), Avenida de Vicent Sos Baynat, s/n, 12071 Castelló de la Plana, Castellón, Spain.

[2]Facultad de Ciencias, Instituto de Ciencias Químicas, Isla Teja, Universidad Austral de Chile, 5090000, Valdivia, Chile.

[3]National Research Council, Institute for Chemical and Physical Processes (CNR-IPCF), Via G. Moruzzi 1, 56124, Pisa, Italy

[4]Department of Chemistry and Industrial Chemistry, University of Pisa, Via G. Moruzzi 13, 56124, Pisa, Italy.

[5]Center of Materials and Nanotechnologies, Faculty of Chemical Technology, University of Pardubice, Nam. Cs. Legii 565, 53002 Pardubice, Czech Republic.

[6]Central European Institute of Technology, Brno University of Technology, Purkyňova 123,612 00 Brno, Czech Republic.

*Corresponding author: andres.gualdron@uach.cl, sero@uji.es.

Synthesis of $CsPbX_3$ (X = Br, I) perovskite nanocrystals (PNCs)

$CsPbX_3$ PNCs were prepared by a hot-injection synthesis throughout mixing both the Cs-oleate and PbX_2 solutions in stoichiometric amounts with some modifications. To prepare the Cs-oleate solution, 0.407 g Cs_2CO_3 (202126, 99.9 %, Sigma-Aldrich) and 1.8 mL oleic acid (OA, 364525, 90 %, Sigma-Aldrich) and 20 mL of 1-octadecene (1-ODE, O806, 90 %, Sigma-Aldrich) were mixed into a 50 mL-three neck flask, stirred vigorously under vacuum for 30 min at 80 ºC. The temperature was increased to 120 ºC and kept under vacuum for 30 min. The mixture was heated at 150 °C under N_2 atmosphere, until complete Cs_2CO_3 dissolution. The resultant transparent solution was kept at 120 °C to avoid the Cs_2O precipitation from Cs-oleate.

For the synthesis of $CsPbX_3$, 1.0 g $PbBr_2$ (ABCR; AB202085, 99.998%) (1.0 g PbI_2 (ABCR; AB111058, 99.999%)) and 50 mL 1-ODE were put into a 100 mL-three neck flask and degasified at 120 °C for 1 h under stirring. Then, 5.0 mL of each preheated OA and oleylamine (HT-OA100, 98 %, Sigma-Aldrich) were added to the flask to promote the PbX_2 dissolution. Then, the temperature of PbX_2 mixture was rapidly increased to reach 170-180 °C and 4 mL of preheated Cs-oleate was swiftly injected, obtaining a green precipitate in the colloidal solution. The flask was immediately added into

an ice bath for 5 s to quench the reaction mixture. To isolate the final product, PNCs were centrifuged at 5000 for 5 min with methyl acetate (MeOAc, 296996, 99.5%, Sigma Aldrich) (30 mL of PNCs liquor washed with 60 mL MeOAc). PNCs pellets were separated from supernatant, redispersed with hexane (CHROMASOLV, 34859, 99.7 %, Honeywell) and stored in the fridge for 24 h. The PNCs solution was centrifuged again at 6500 RPM for 5 min. Here, solvent was removed, and the final product was dissolved again in hexane at a concentration ~60 $mgmL^{-1}$. Then, PNCs colloidal solutions in hexane were added into BuOH (named hereafter as PNCs-BuOH dispersions) in a PNCs:BuOH volume ratio 1:4, in absence and presence of diverse concentrations of didodecyldimethylammonium bromide (DDAB, 359025, 98%, Sigma Aldrich): 4.3, 8.5, 17, 43, 85 and 200 mM.

For the preparation and stabilization of mixed halide $CsPbBr_{3-x}I_x$ PNCs in alcohol medium, two different procedures were conducted: (i) anion-exchange by mixing pure $CsPbBr_3$ and $CsPbI_3$ PNCs solutions in hexane (60 mg mL^{-1}) in a Br:I volume ratio 1:1. The mixture was dispersed in BuOH in presence of 17 mM DDAB. (ii) Addition of different volumes of 200 $mgmL^{-1}$ SrI_2/MeOH solution (up to complete a total volume 350 μL) to $CsPbBr_3$ PNCs-BuOH dispersions in presence of 17 mM and 43 mM DDAB. For stabilizing $CsPbI_3$ PNCs, colloidal solution was added into BuOH in a PNCs:BuOH volume ratio 1:4, in absence and presence of 8.5, 17 and 43 mM DDAB.

Characterization of morphology, structure, optical properties, and surface environment of the $CsPbX_3$ PNCs dispersed in alcohol media

The morphology of the PNCs was analyzed through high-resolution transmission electron microscopy (HRTEM) images by using a field emission tunneling electron microscope (FE-TEM, Hitachi HF-3300, with applied bias of 300 kV. Scanning Electron microscopy measurements were carried out by using a JSM7001F microscope. The average particle size of PNCs was obtained from the TEM images with ImageJ software. Here, prepared dispersions were studied in three different conditions as follows: (i) fresh PNCs-BuOH samples at 0 h, (ii) 48 h and (iii) 5040 h of aging after adding MeOH to complete a total added volume up to 600 μL. PNCs were aged by exposing them to ambient air at room temperature (~25 ºC), and 60% relative humidity under light room conditions.

The crystalline structure for the PNCs was studied through selective area electron diffraction (SAED) patterns and obtaining the corresponding X-ray diffraction (XRD) profiles. A D4 Endeavor diffractometer from Bruker-AXS was used, using a Cu Kα radiation source (λ = 1.54056 Å) with following factors: 2θ range of 5°-80° (0.02 °/step and 1.2 s/step). UV-vis absorption spectra were acquired by using a UV-vis absorption spectrophotometer (Varian, Cary 300). The wavelength range for the measurements was 400–850 nm. Steady state- and time-resolved photoluminescence (PL) measurements were conducted through photoluminescence spectrophotometer (Fluorolog 3-11, Horiba). An excitation wavelength of 420 nm was used to perform the steady state PL. The concentration of the samples was fixed to 2 $mgmL^{-1}$ in hexane, using a quartz cuvette of 10 x 10 mm. Time-resolved PL measurements were performed at 405 nm pulsed laser (NanoLED-405L, <100 ps of

pulse width, 1 MHz frequency). The absolute photoluminescence quantum yield (PLQY) of the PNCs dispersions was estimated through a Hamamatsu Absolute PLQY Measurement System C9920-02, equipped with an integrating sphere, at an excitation wavelength of 400 nm. Here, absorbance was adjusted in an interval range around 0.5-0.7 to conduct the measurements, being these values suitable to achieve the maximum PLQY in the samples. For stability measurements, optical features of $CsPbBr_3$-BuOH dispersions with different DDAB content were studied in absence and presence of MeOH. PL spectra of PNCs-BuOH dispersions were acquired at 0 and 1 h without MeOH. Then, volumes of 100 and 200 μL of MeOH were added to PNCs-BuOH samples from 2 to 6 h (at times intervals of 1 h) to achieve a total volume of 600 μL of MeOH. The resultant dispersions were analyzed at different times to achieve a maximum of 5040 h. In the case of $CsPbBr_{3-x}I_x$ (anion-exchanged by SrI_2) and $CsPbI_3$ PNCs, stability was studied through PL measurements for 6 h.

Surface chemical composition and electronic state of PNCs were determined by X-ray Photoelectron Spectroscopy (XPS, ESCA-2R, Scienta-Omicron). Spectra were recorded using monochromatic Al Kα = 1486.6 eV. The following sequence of spectra were recorded: survey spectra, C 1s, Pb 4f, I 3d, Cl 2p Br 3d, O 1s, N 1s and C 1s again to verify the stability of the charge as the function of time. The survey and high-resolution spectra were recorded at a pass energy of 150 and 20 eV, respectively. Binding energy scale was referenced to adventitious carbon (284.8 eV). CasaXPS processing software (Casa software Ltd) was used to analyze the data and the quantitative analysis was made using sensitivity factors provided by the manufacturer. Then, NMR measurements were carried out on a Varian INOVA600 spectrometer equipped with a 5 mm probe operating at 600 MHz for ^1H nuclei; the temperature was controlled to ± 0.1°C. The proton spectra were acquired with the minimum spectral width required. Samples in toluene-d_8 were analyzed by using 3 s of relaxation delay, a 60° pulse of 6.03 μs, 64 scans and a gain of 4. The FID was acquired into 64 K data points during a 3.418 s acquisition time, and data were processed with 1.0 Hz line broadening. All deuterated solvents (toluene-d_8, $CDCl_3$, methanol-d_3) were purchased from Deutero GmbH (Kastellaun, Germany).

Theoretical calculations

The ligand exchange processes occurring on the facets of the cubic $CsPbBr_3$ nanocrystals have been further investigated by density functional theory calculations. For this purpose, surfaces of $CsPbBr_3$ perovskite semiconductor with attached ligands and Br vacancies, namely oleate, OLAm, DDAB, MeO^-, and BuO^- ligands, were suggested and computed with DFT. These surfaces of interest belong to slabs of thickness ~12 Å which were computed with the DFT code CP2K,[1, 2] a software package which mixes plane waves and Gaussian functions. For the computations, we used the Perdew-Burke-Ernerhof (PBE) approach to generate the pseudopotentials,[3] a double-zeta valence basis set augmented with polarized functions (DZVP), and spin polarization. To properly reach the ground states, the atomic positions in the slabs were geometrically relaxed until the forces on the individual

nuclei became smaller than 0.001 Ha/a_0, where a_0 is the Bohr radius. Furthermore, to minimize the intrinsic interactions related to the supercell approximation, neighbouring slabs were separated from each other by a suitable void space of 12 Å, and dipolar corrections were included. From the DFT total energies obtained for the suggested input and output $CsPbBr_3$ geometries, we could positively characterize ligand exchange processes occurring on the facets of cubic PNCs decorated with attached molecules of interest.

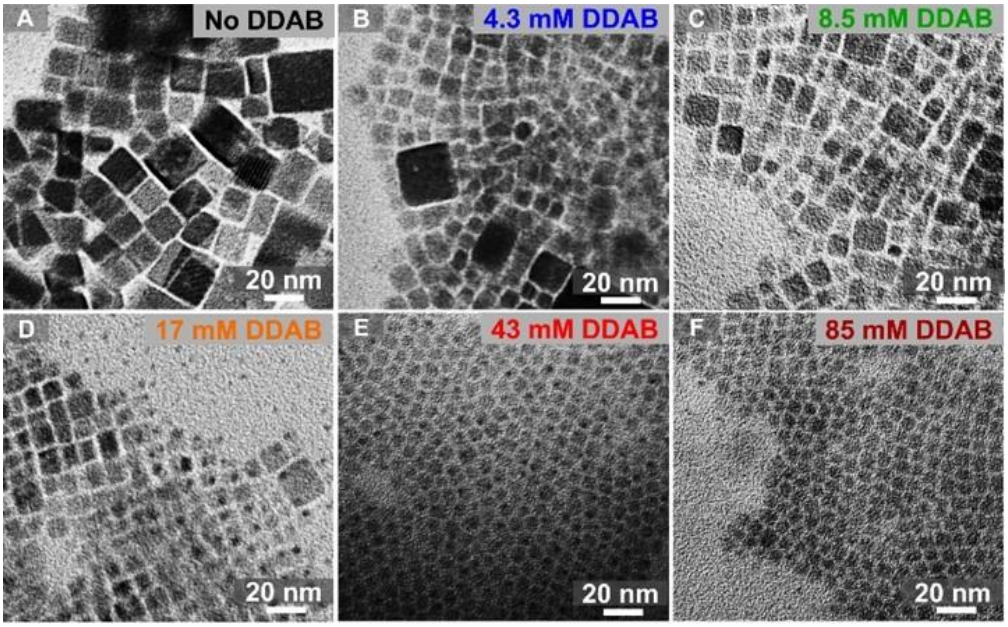

Figure S1. TEM images of $CsPbBr_3$ PNCs dispersed in MeOH/BuOH system at 48 h aging, in (A) absence and presence of (B) 4.3 mM, (C) 8.5 mM, (D) 17 mM, (E) 43 mM and (F) 85 mM DDAB.

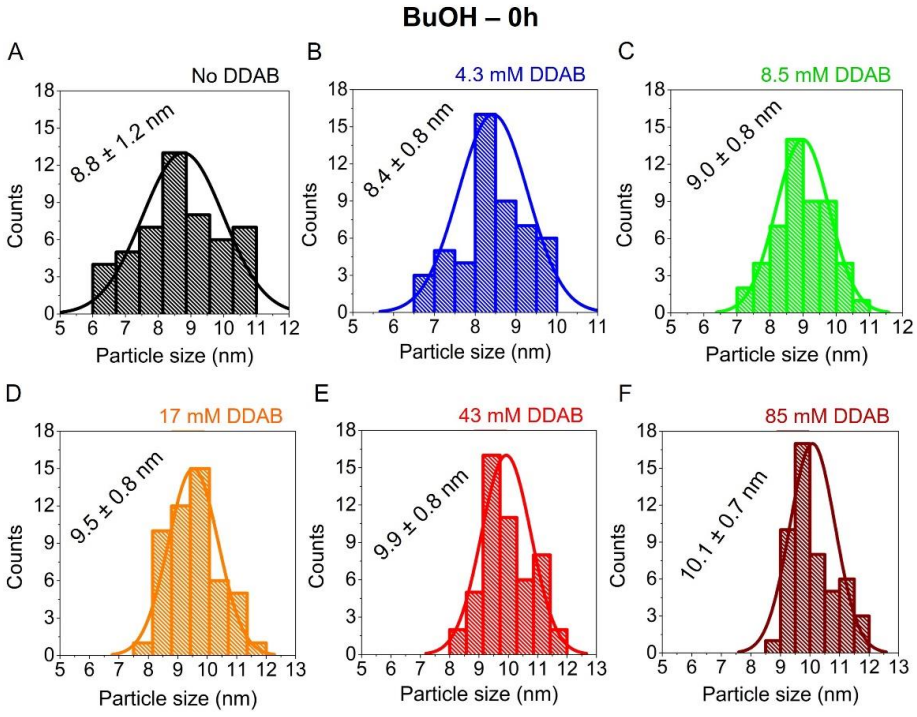

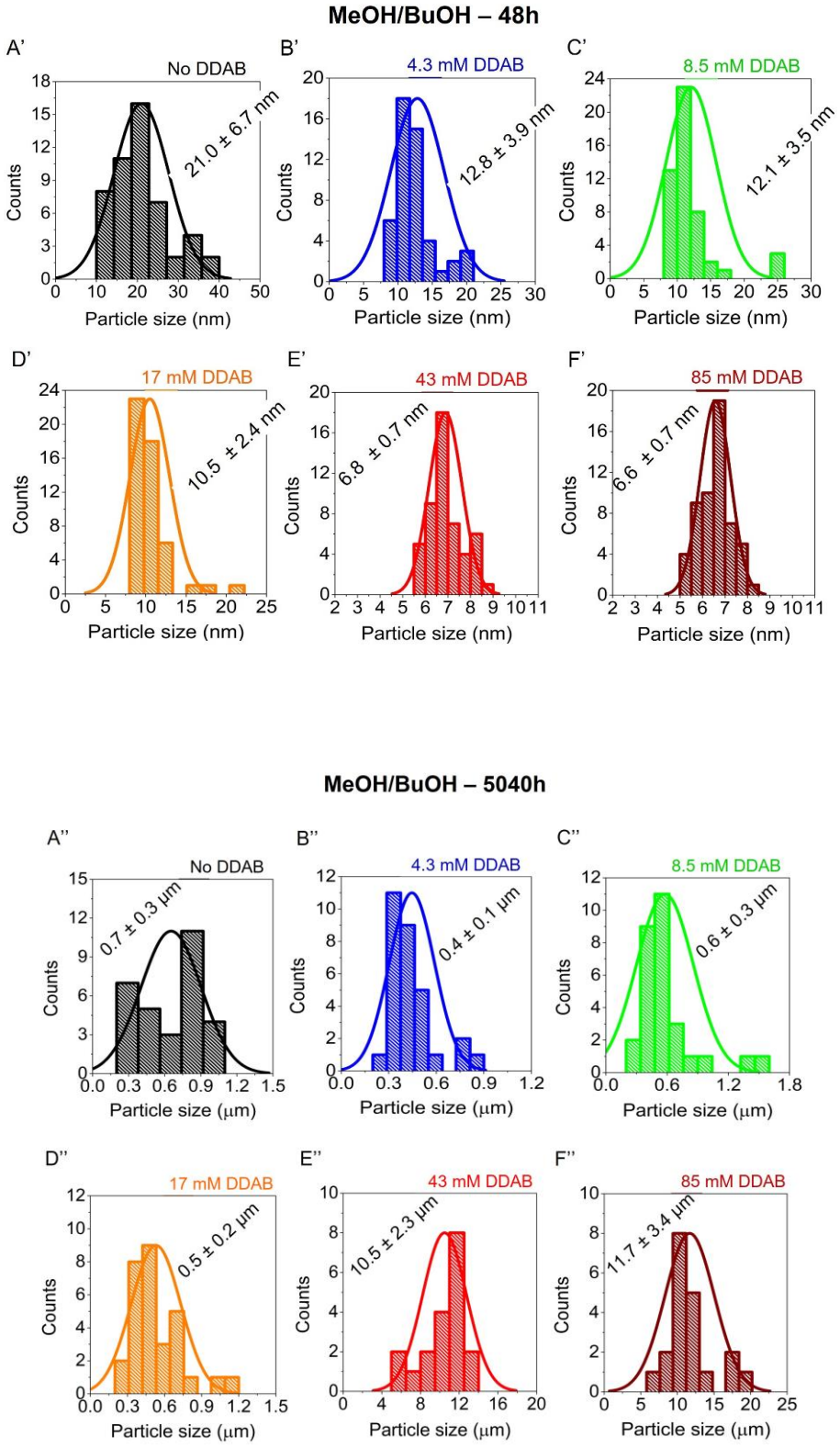

Figure S2. Histograms for estimating the particle size of $CsPbBr_3$ PNCs dispersed into (A-F) BuOH at 0 h, (A'-F') MeOH/BuOH after 48 h aging and (A''-F'') MeOH/BuOH after 5040 h aging (A, A',

A'') in absence and presence of (B, B', B'') 4.3 mM, (C, C', C'') 8.5 mM, (D, D', D'')17 mM, (E, E', E'') 43 mM and (F, F', F'') 85 mM DDAB.

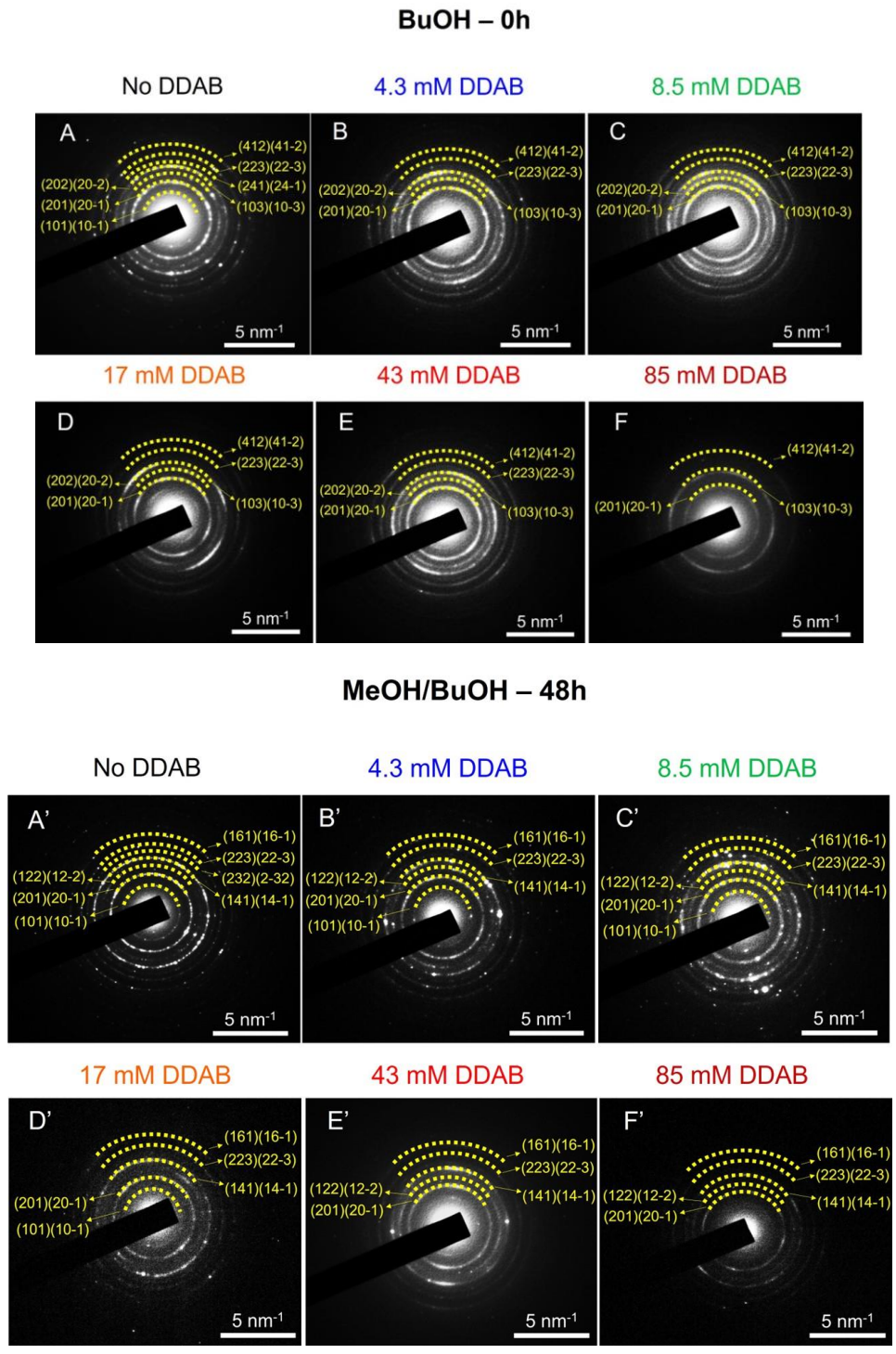

Figure S3. SAED patterns obtained for $CsPbBr_3$ PNCs dispersed in (A-F) BuOH at 0 h, (A'-F') MeOH/BuOH after 48 h aging (A, A') in absence and presence of (B, B') 4.3 mM, (C, C') 8.5 mM, (D, D')17 mM, (E, E') 43 mM and (F, F') 85 mM DDAB.

Table S1. Chemical composition of as-prepared $CsPbBr_3$ PNCs dispersed in BuOH at 0 h, in absence and presence of different DDAB concentrations, estimated from EDS.

DDAB concentration	Composition obtained from EDS			
	Cs (at.%)	Pb (at.%)	Br (at.%)	Br/Pb ratio
No DDAB	19.23	19.17	61.60	3.21
4.3 mM	18.83	18.44	62.73	3.40
8.5 mM	18.46	18.33	63.21	3.45
17 mM	18.26	18.28	63.45	3.47
43 mM	17.17	17.09	65.74	3.85
85 mM	15.82	15.49	68.69	4.43

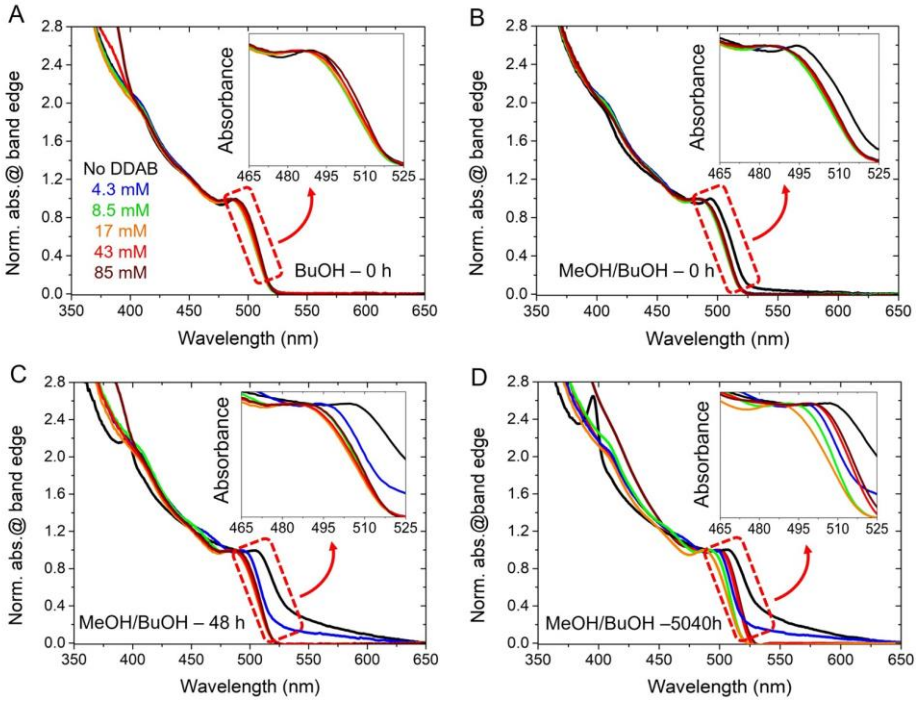

Figure S4. UV-vis absorption spectra of $CsPbBr_3$ PNCs dispersed in (A) BuOH at 0 h, and MeOH/BuOH at (B) 0 day, (C) 48 h and (D) 5040 h, by varying the DDAB concentration. Inset of figures exhibit a zoom of the absorption edges of each PNCs sample under the above polar environment/time conditions.

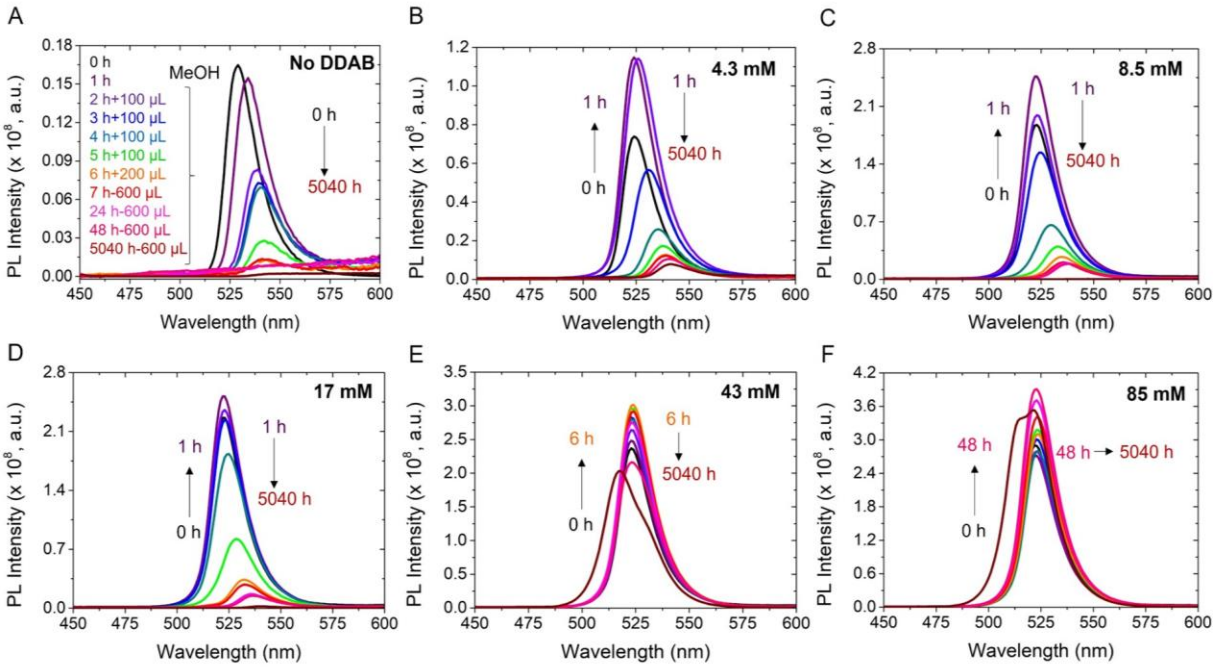

Figure S5. PL spectra of $CsPbBr_3$ PNCs dispersed in BuOH and MeOH/BuOH systems, by varying the aging time, (A) in absence and presence of (B) 4.3 mM, (C) 8.5 mM, (D)17 mM, (E) 43 mM and (F) 85 mM DDAB.

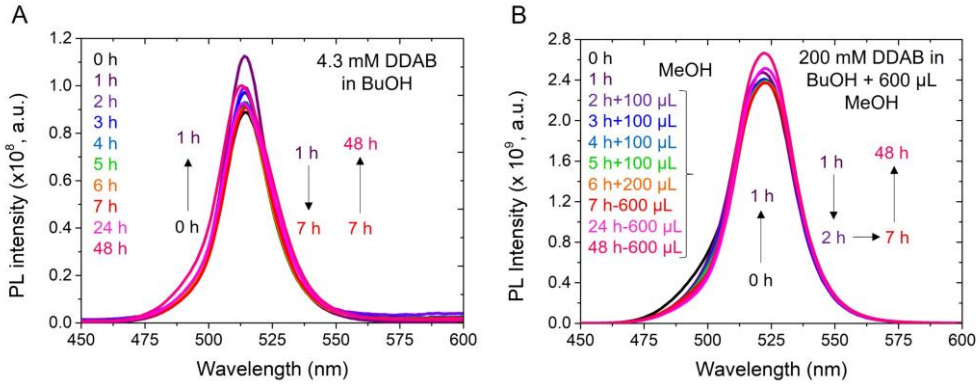

Figure S6. PL spectrum of $CsPbBr_3$ PNCs dispersed in BuOH by varying the aging time, in presence of (A) 4.3 mM DDAB, and (B) 200 mM DDAB in MeOH/BuOH medium. Controlled volumes of MeOH were added to PNCs-BuOH dispersions from 2 to 6 h (at times intervals of 1 h) to reach a total added volume of 600 µL of MeOH.

XRD characterization of $CsPbBr_3$ PNCs dispersed in alcohol media at different DDAB concentration/aging time

To obtain a deeper understanding about the role of DDAB content on the crystalline phase of PNCs into the alcohol systems in function of time, we obtained X-ray diffraction (XRD) measurements, as seen in Figures S7A-D. We led the XRD patterns of PNCs samples dispersed in

BuOH at 0 h, and MeOH/BuOH at 0 h, 48 h and 5040 h, deposited on glass substrates and dried under ambient air, where important structural transformations were noted. In all the scenarios, perovskite samples in the absence and presence of 4.3 mM DDAB show the typical XRD profile of the $CsPbBr_3$ orthorhombic phase (ICSD 97851),[4] being in good accordance with SAED patterns. Nevertheless, by increasing the ligand concentration in the polar environment, the peaks of $CsPbBr_3$ are gradually vanished in both BuOH and MeOH/BuOH systems at 0 h, while new peaks emerged, matching with two different crystalline systems: 2D $CsPb_2Br_5$ (ICSD 254290)[5] and 0D Cs_4PbBr_6 (ICSD 162158)[6] perovskites. Unlike the 3D $CsPbBr_3$ structure, which is composed by corner-sharing $[PbBr_6]^{4-}$ octahedra and Cs^+ species filling voids formed by four $[PbBr_6]^{4-}$ units, 0D Cs_4PbBr_6 shows a $PbBr_2$-deficient structure, where $[PbBr_6]^{4-}$ octahedra are fully decoupled.[6, 7] Attending to the fact that DDAB mediates the partial exfoliation of PNCs surface, releasing $[PbBr_6]^{4-}$ octahedra and forming DDAB-Pb based complexes in solution,[8] it is deductible that part of $PbBr_2$ needed to maintain the 3D perovskite structure is extracted. In this context, the structural reorganization is facilitated to start the 3D-to-0D transformation, through the following reaction: $4CsPbBr_3 \rightarrow Cs_4PbBr_6 + 3PbBr_2$.[6]

Conversely, the aging of PNCs into the alcohol environment after 48 and 5040 h hinders the 3D-to-0D transformation, observing lower intense XRD signals from Cs_4PbBr_6 crystalline phase, in combination with the characteristic peaks from 3D structure. Here, typical signals from 2D $CsPb_2Br_5$ are not evidenced. This fact can indicate that PNCs exfoliation has been delayed (presumably DDAB has reached an equilibrium between surface passivation-exfoliation), making that lesser $[PbBr_6]^{4-}$ units are extracted from $CsPbBr_3$ nanocubes. The structural transformation can also be observed by analyzing the XRD peak ~15.4º in all the above scenarios, which depict a doublet associated to the perovskite assembly to generate an ordering structure (Figures S7A'-D'). In absence of DDAB, this structure is related to highly defective bulk-like $CsPbBr_3$ crystals. Then, by increasing the ligand content in BuOH and BuOH + MeOH media at 0 h, the XRD doublet disappears, and a single peak emerges at higher Bragg angles. This change is ascribed to perovskite lattice compression, reinforcing the hypothesis about the $[PbBr_6]^{4-}$ removal from PNCs surface. However, this process is restrained by aging the perovskite samples in the alcohol environment, depicting the XRD doublet along the different DDAB concentrations. In line with this observation, a shift in the signal to lower Bragg angles was seen after 48 h-aging, and no changes in the doublet position was detailed after 5040 h-aging. In the light of the outcome exposed here, we conclude that the small PNCs are the building blocks to prepare bigger crystals mediated by DDAB passivation. This confirms that nanocrystal assemblies make more stable the perovskite system to the polar solvent. Lastly, the structural reorganization explained above occurs when the polar solvent is volatilized to prepare the XRD samples, allowing to reinforce the hypothesis that alcohol itself also plays an important role on the PNCs stabilization.

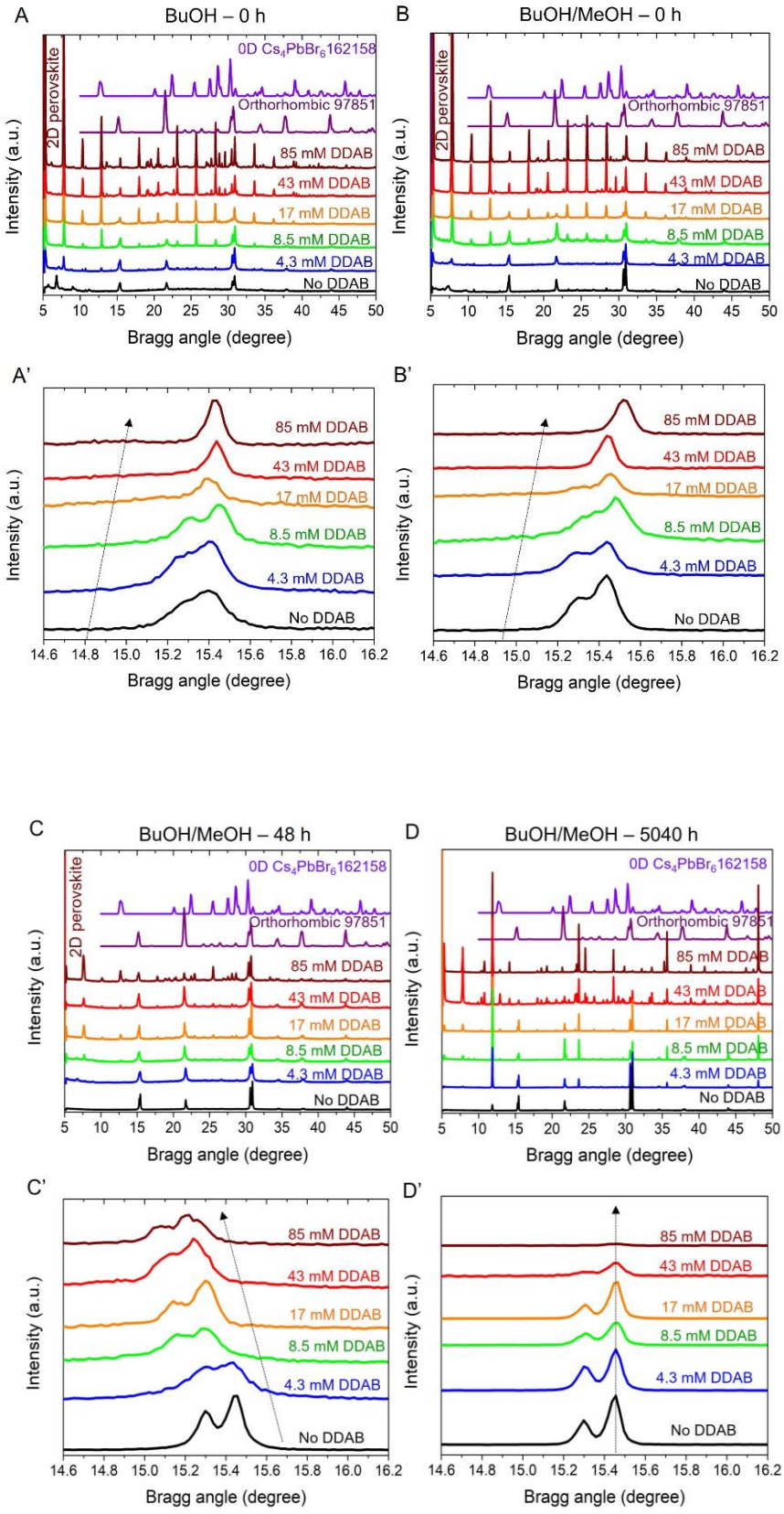

Figure S7. XRD patterns obtained for $CsPbBr_3$ PNCs dispersed in (A,A') BuOH at 0 h, and (B,B') MeOH/BuOH at 0 h, (C,C') 48 h and (D,D') 5040 h, by varying the DDAB concentration.

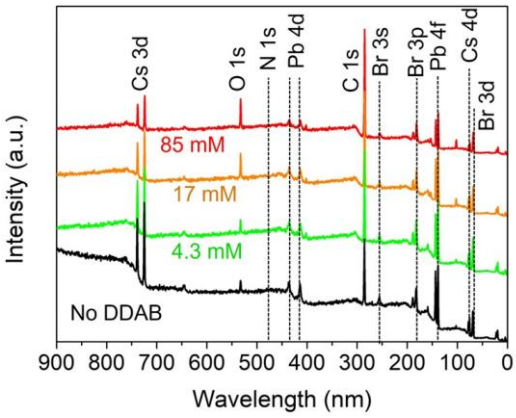

Figure S8. XPS survey spectra of $CsPbBr_3$ PNCs dispersed in BuOH at 0 h, by varying the DDAB concentration.

Table S2. Chemical atomic composition of as-prepared $CsPbBr_3$ PNCs dispersed in BuOH at 0 h, in absence and presence of different DDAB concentrations obtained by XPS.

DDAB concentration	C (at.%)	O (at.%)	Pb (at.%)	Br (at.%)	Cs (at.%)	N (at.%)	Br/Pb	$O_{total}/(Br+O_{total})$	$O_{total}/(Pb+O_{total})$
No DDAB	70.88	5.20	4.85	12.96	3.68	2.43	2.67	0.26	0.48
4.3 mM	74.86	4.92	3.19	10.32	3.71	3.00	3.23	0.32	0.61
17 mM	75.38	8.49	2.79	8.50	2.77	2.06	3.05	0.50	0.75
85 mM	80.47	8.36	1.55	5.65	1.64	2.32	3.65	0.60	0.84

^{1}H-NMR characterization of $CsPbBr_3$ dispersions in alcohol by varying the DDAB content[9, 10]

With the purpose to obtain information about the surface chemistry of $CsPbBr_3$ PNCs into alcohol media in absence and presence of DDAB, materials were characterized through proton (^{1}H) NMR (Nuclear Magnetic Resonance) spectroscopy. First, a portion of the colloidal solution of PNCs in hexane was dried and dissolved in toluene-d_8. The corresponding ^{1}H NMR spectrum is shown in Figure S9A, where a weak signal centred at δ = 3.04 ppm is found, which is in accordance with the presence of negligible (around 3 wt %) amounts of *N*-oleyloleamide (NOA), arising from the reaction between oleic acid (OA) and oleylamine (OLA). This signal is associated to the methylene unit in α-position with respect to the amide group. The NMR analysis also pointed out a residual content of 1-octadecene (1-ODE) that was employed as solvent in the synthetic procedure.

Knowing that the evaluation of the capping organic ligands concentration is an important aspect in PNCs characterization, the total amount of OLA and OA was calculated with respect to 1-ODE by integrating the signals at δ = 5.70-5.40 ppm (Figure S9A), belonging to the olefinic protons of the ligands; the content of 1-ODE was determined by using as external standard a solution of 1-ODE at known concentration. The relative OLA/OA molar ratio then was calculated as 1:1 based on the destructive ligand composition analysis: according to the procedure,[11] PNCs were dissolved in DMSO-d_6 and 5 μL of trifluoroacetic acid (TFA) were added. Based on the results of the analyses, OLA and OA were estimated around 11 wt % each with respect to the total PNCs content.

It is noteworthy that the olefinic region depicted in Figure S9A (black spectrum) is characterized by broad signals, indicative of an interaction between both ligands and the PNCs surface. When the ligands are mixed without PNCs (orange spectrum in Figure S9A), these resonances are resolved, and it is possible to distinguish the signal belonging to OLA, centred at δ = 5.47 ppm, from that belonging to OA, at δ = 5.45 ppm. On the contrary, when the ligands are bound to PNCs (black spectrum in Figure S9A), OLA and OA resonances shift at δ = 5.53 ppm and 5.47 ppm respectively, the former being more affected by the interaction with the perovskite. By analysing the NMR resonances of pure DDAB, signals located at δ = 3.45 and 3.55 are ascribed to methylene and methyl protons near to NH_3^+ functionality, respectively (green spectrum in Figure S9A), and the co-existence of OA and OLA ligands causes a shift at lower frequencies for these resonances (red spectrum in Figure S9A). A possible interaction between OLA/OA and DDAB is responsible of the displacement in the DDAB peak positions, which is also deduced from the appearance of the NMR signals of free OLA and OA.

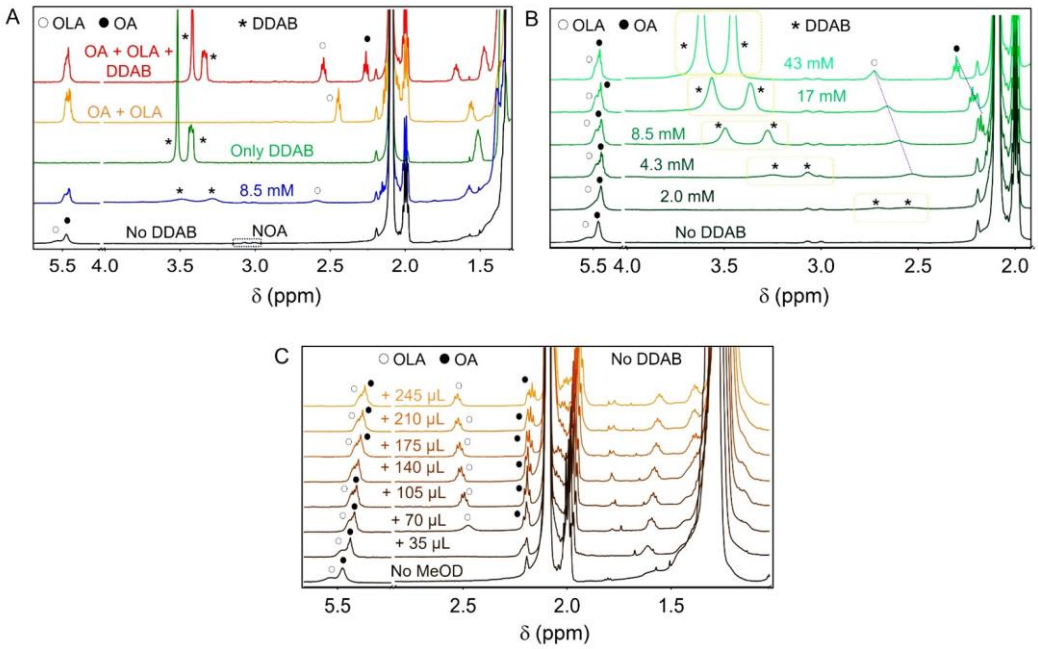

Figure S9. (A) ^{1}H (600 MHz, toluene-d_8, 298 K) NMR spectra of $CsPbBr_3$ PNCs colloidal solutions, in absence (black) and presence (blue) of DDAB. Characteristic NMR resonances of capping ligand samples, DDAB (green), OLA+OA (orange), and OLA+OA+DDAB mixtures (red), were also obtained for comparative purposes. (B) ^{1}H (600 MHz, toluene-d_8, 298 K) NMR spectra of PNCs colloidal solutions titrated with DDAB. (C) ^{1}H (600 MHz, toluene-d_8, 298 K) NMR spectra of PNCs in absence of DDAB, titrated with deuterated methanol (MeOD).

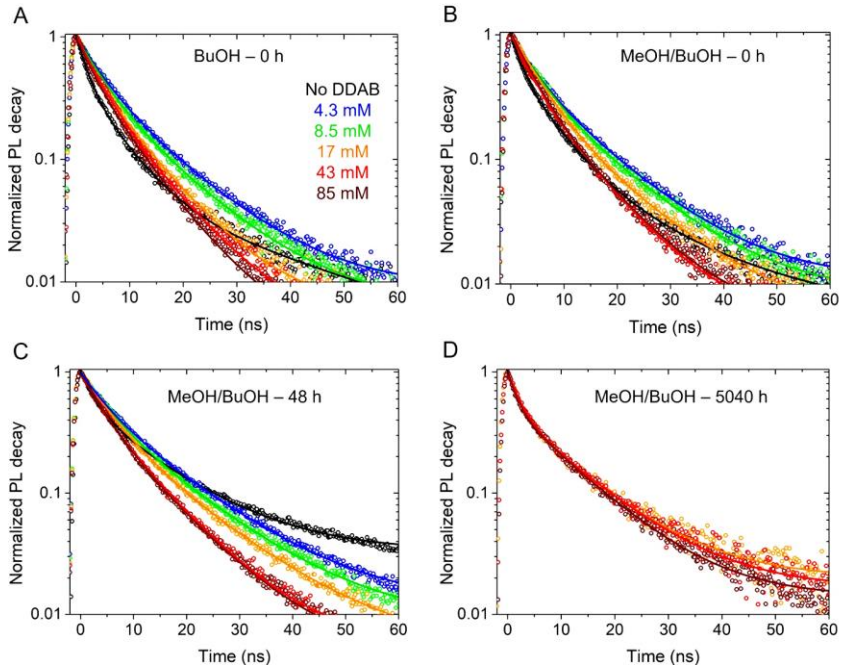

Figure S10. Time-resolved PL decay measurements of (A) BuOH at 0 h, and (B) MeOH/BuOH at 0 day, (C) 48 h and (D) 5040 h, by varying the DDAB concentration. Solid lines correspond to fitting the PL decays through a bi-exponential equation, $\mathrm{PL} = y_0 + A_1 e^{-x/\tau_1} + A_2 e^{-x/\tau_2}$.

Table S3. Determination of radiative and non-radiative recombination decay rate constants, k_r and k_{nr}, respectively by fitting the time-resolved PL decays of $CsPbBr_3$ dispersed in BuOH at 0 h aging, by varying the DDAB concentration shown in Figure S10A to a bi-exponential function $\mathrm{PL} = y_0 + A_1 e^{-x/\tau_1} + A_2 e^{-x/\tau_2}$.[12] Expressions used in the calculations: $\tau_{avg} = (\Sigma A_i \tau_i^2 / \Sigma A_i \tau_i)$, $\tau_{avg} = 1/(k_r + k_{nr})$ and $k_r = (\mathrm{PLQY}/\tau_{avg})$.[13] PLQY values were used in 0-1 range.

DDAB concentration	A_1 (%)	τ_1 (ns)	A_2 (%)	τ_2 (ns)	PLQY	τ_{avg} (ns)	k_r (10^8 s^{-1})	k_{nr} (10^8 s^{-1})	k_{nr}/k_r
No DDAB	0.383	2.73	0.612	11.31	0.41	8.02	0.511	0.735	1.439
4.3 mM	0.480	5.42	0.520	16	0.73	10.09	0.668	0.246	0.370
8.5 mM	0.513	5.29	0.487	15.34	1.00	10.02	0.982	0	0
17 mM	0.510	5.10	0.490	14.74	1.00	9.82	1.02	0	0
43 mM	0.567	4.45	0.433	11.53	1.00	7.52	1.33	0	0
85 mM	0.581	4.26	0.419	11.38	1.00	7.24	1.38	0	0

Table S4. Determination of radiative and non-radiative recombination decay rate constants, k_r and k_{nr}, respectively by fitting the time-resolved PL decays of $CsPbBr_3$ dispersed in MeOH/BuOH at 0 h aging, by varying the DDAB concentration shown in Figure S10B to a bi-exponential function $\mathrm{PL} = y_0 + A_1 e^{-x/\tau_1} + A_2 e^{-x/\tau_2}$.[12] Expressions used in the calculations: $\tau_{avg} = (\Sigma A_i \tau_i^2 / \Sigma A_i \tau_i)$, $\tau_{avg} = 1/(k_r + k_{nr})$ and $k_r = (\mathrm{PLQY}/\tau_{avg})$.[13] PLQY values were used in 0-1 range.

DDAB	A_1	τ_1	A_2	τ_2	PLQY	τ_{avg}	k_r	k_{nr}	k_{nr}/k_r

concentration	(%)	(ns)	(%)	(ns)		(ns)	(10^8 s^{-1})	(10^8 s^{-1})	
No DDAB	0.326	3.02	0.674	11.33	0.37	8.62	0.429	0.731	1.703
4.3 mM	0.406	5.11	0.594	15.14	0.78	11.11	0.705	0.199	0.282
8.5 mM	0.453	5.15	0.547	14.86	1.00	10.50	0.956	0	0
17 mM	0.492	4.79	0.508	12.93	1.00	8.93	1.12	0	0
43 mM	0.510	4.32	0.490	11.04	1.00	7.61	1.31	0	0
85 mM	0.502	4.23	0.498	10.97	1.00	7.59	1.32	0	0

Table S5. Determination of radiative and non-radiative recombination decay rate constants, k_r and k_{nr}, respectively by fitting the time-resolved PL decays of $CsPbBr_3$ dispersed in MeOH/BuOH at 48 h aging, by varying the DDAB concentration shown in Figure S10C to a bi-exponential function $\mathrm{PL} = y_0 + A_1 e^{-x/\tau_1} + A_2 e^{-x/\tau_2}$.[12] Expressions used in the calculations: $\tau_{avg} = (\Sigma A_i \tau_i^2 / \Sigma A_i \tau_i)$, $\tau_{avg} = 1/(k_r + k_{nr})$ and $k_r = (\mathrm{PLQY}/\tau_{avg})$.[13] PLQY values were used in 0-1 range.

DDAB concentration	A_1 (%)	τ_1 (ns)	A_2 (%)	τ_2 (ns)	PLQY	τ_{avg} (ns)	k_r (10^8 s^{-1})	k_{nr} (10^8 s^{-1})	k_{nr}/k_r
No DDAB	0.263	3.71	0.737	16.62	0.07	13.22	0.053	0.703	13.29
4.3 mM	0.350	5.77	0.650	17.06	0.21	13.11	0.206	0.557	2.704
8.5 mM	0.420	5.85	0.580	16.88	0.63	12.25	0.051	0.302	0.587
17 mM	0.442	5.56	0.558	14.99	0.87	10.82	0.804	0.120	0.149
43 mM	0.511	4.83	0.489	12.81	1.00	8.73	1.15	0	0
85 mM	0.502	4.83	0.498	12.81	1.00	8.80	1.14	0	0

Table S6. Determination of radiative and non-radiative recombination decay rate constants, k_r and k_{nr}, respectively by fitting the time-resolved PL decays of $CsPbBr_3$ dispersed in MeOH/BuOH at 5040 h aging, by adding 17, 43 and 85 mM shown in Figure S10D to a bi-exponential function $\mathrm{PL} = y_0 + A_1 e^{-x/\tau_1} + A_2 e^{-x/\tau_2}$.[12] Expressions used in the calculations: $\tau_{avg} = (\Sigma A_i \tau_i^2 / \Sigma A_i \tau_i)$, $\tau_{avg} = 1/(k_r + k_{nr})$ and $k_r = (\mathrm{PLQY}/\tau_{avg})$.[13] PLQY values were used in 0-1 range.

DDAB concentration	A_1 (%)	τ_1 (ns)	A_2 (%)	τ_2 (ns)	PLQY	τ_{avg} (ns)	k_r (10^8 s^{-1})	k_{nr} (10^8 s^{-1})	k_{nr}/k_r
17 mM	0.244	3.02	0.756	13.40	0.08	10.86	0.074	0.847	11.50
43 mM	0.204	2.68	0.796	13.08	0.78	10.95	0.712	0.201	0.282
85 mM	0.187	2.37	0.813	12.36	0.93	10.49	0.886	0.067	0.075

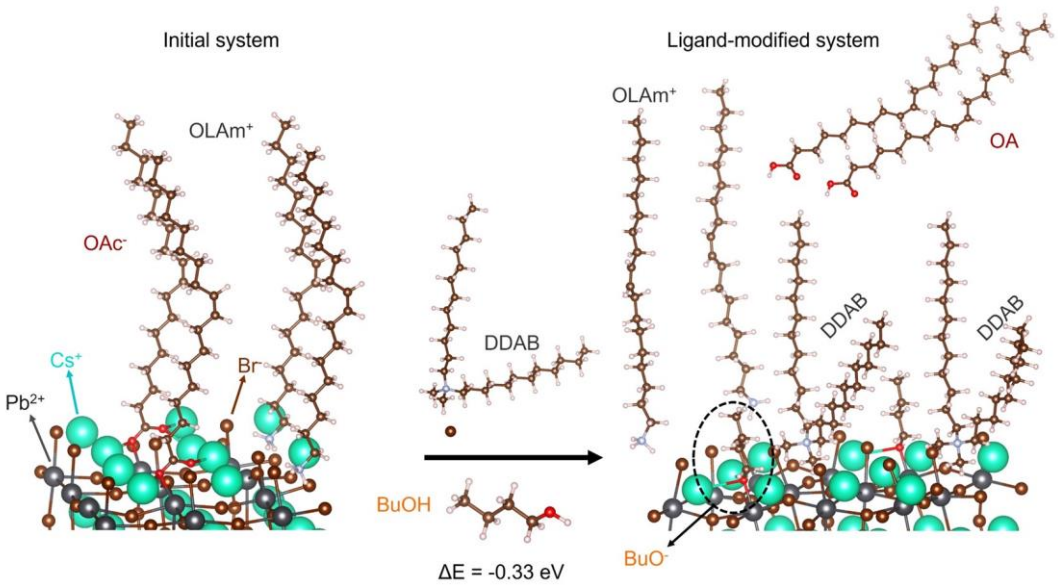

Figure S11. Schematic representation of the ligand passivation of $CsPbBr_3$ PNCs surface conducted by DDAB in presence of BuOH medium. DDA^+, $OLAm^+$, Br^- and BuO^- species are responsible to produce the protection coverage on perovskite surface.

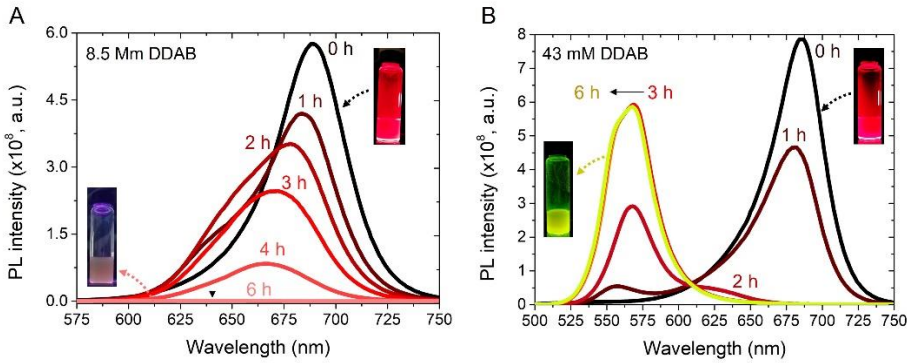

Figure S12. Time-dependent PL spectra of $CsPbI_3$ PNCs dispersed in BuOH at 0 h in presence of (A) 8.5 mM and (B) 43 mM DDAB.

References

[1] J. Hutter, M. Iannuzzi, F. Schiffmann, J. VandeVondele, *Wiley Interdisciplinary Reviews: Computational Molecular Science* **2014**, 4, 15.

[2] C. Giansante, I. Infante, *The Journal of Physical Chemistry Letters* **2017**, 8, 5209.

[3] J. P. Perdew, K. Burke, M. Ernzerhof, *Physical Review Letters* **1996**, 77, 3865.

[4] J. Liu, K. Song, Y. Shin, X. Liu, J. Chen, K. X. Yao, J. Pan, C. Yang, J. Yin, L.-J. Xu, H. Yang, A. M. El-Zohry, B. Xin, S. Mitra, M. N. Hedhili, I. S. Roqan, O. F. Mohammed, Y. Han, O. M. Bakr, *Chemistry of Materials* **2019**, 31, 6642.

[5] S. Lou, Z. Zhou, T. Xuan, H. Li, J. Jiao, H. Zhang, R. Gautier, J. Wang, *ACS Applied Materials & Interfaces* **2019**, 11, 24241.

[6] Z. Liu, Y. Bekenstein, X. Ye, S. C. Nguyen, J. Swabeck, D. Zhang, S.-T. Lee, P. Yang, W. Ma, A. P. Alivisatos, *Journal of the American Chemical Society* **2017**, 139, 5309.
[7] Y. Li, H. Huang, Y. Xiong, S. V. Kershaw, A. L. Rogach, *CrystEngComm* **2018**, 20, 4900.
[8] S. K. Balakrishnan, P. V. Kamat, *Chemistry of Materials* **2017**, 30, 74.
[9] E. Hassanabadi, M. Latifi, A. F. Gualdrón-Reyes, S. Masi, S. Y. joon, M. Poyatos, B. Julián-López, I. Mora Seró, *Nanoscale* **2020**, 12, 14194.
[10] M. Imran, P. Ijaz, L. Goldoni, D. Maggioni, U. Petralanda, M. Prato, G. Almeida, I. Infante, L. Manna, *ACS Energy Letters* **2019**, 4, 819.
[11] D. Baranov, G. Caputo, L. Goldoni, Z. Dang, R. Scarfiello, L. De Trizio, A. Portone, F. Fabbri, A. Camposeo, D. Pisignano, L. Manna, *Chemical Science* **2020**, 11, 3986.
[12] M. I. Bodnarchuk, S. C. Boehme, S. ten Brinck, C. Bernasconi, Y. Shynkarenko, F. Krieg, R. Widmer, B. Aeschlimann, D. Günther, M. V. Kovalenko, I. Infante, *ACS Energy Letters* **2018**, 4, 63.
[13] C. Lee, Y. Shin, A. Villanueva-Antolí, S. Das Adhikari, J. Rodriguez-Pereira, J. M. Macak, C. A. Mesa, S. Giménez, S. J. Yoon, A. F. Gualdrón-Reyes, I. Mora-Seró, *Chemistry of Materials* **2021**, 33, 8745.